# A Novel Type of Monoheme Cytochrome *c*: Biochemical and Structural Characterization at 1.23 Å Resolution of *Rhodothermus marinus* Cytochrome *c*[†,‡]

Meike Stelter,[§,⊥] Ana M. P. Melo,[§,⊥,||,¶] Manuela M. Pereira,[§] Cláudio M. Gomes,[§] Gudmundur O. Hreggvidsson,[▽] Sigridur Hjorleifsdottir,[▽] Lígia M. Saraiva,[§] Miguel Teixeira,[§] and Margarida Archer[§,*]

*Instituto de Tecnologia Química e Biológica, Universidade Nova de Lisboa, 2780-157 Oeiras, Portugal, Faculdade de Engenharia e Ciências Naturais, Universidade Lusófona de Humanidades e Tecnologias, 1749-024 Lisboa, Portugal, Eco-Bio, Instituto de Investigação Científica Tropical, 2784-505 Oeiras, Portugal, and Prokaria Ltd., 112 Reykjavik, and University of Iceland, 101 Reykjavik, Iceland*

*Received May 27, 2008; Revised Manuscript Received September 8, 2008*

ABSTRACT: Monoheme cytochromes of the C-type are involved in a large number of electron transfer processes, which play an essential role in multiple pathways, such as respiratory chains, either aerobic or anaerobic, and the photosynthetic electron transport chains. This study reports the biochemical characterization and the crystallographic structure, at 1.23 Å resolution, of a monoheme cytochrome *c* from the thermohalophilic bacterium *Rhodothermus marinus*. In addition to an α-helical core folded around the heme, common for this type of cytochrome, the X-ray structure reveals one unusual α-helix and a unique N-terminal extension, which wraps around the back of the molecule. Based on a thorough structural and amino acid sequence comparison, we propose *R. marinus* cytochrome *c* as the first characterized member of a new class of C-type cytochromes.

Monoheme cytochromes of the C-type are very well-studied proteins involved in the electron transport chains of prokaryotes and mitochondria, namely, carrying the electrons from the $bc_1$ complexes or their analogs to heme−copper oxygen reductases, as part of the oxidative phosphorylation process. These electron carriers also participate in the electron transfer chain of photosynthesis. In eukaryotes, the study of the mitochondrial cytochrome *c* has assumed particular relevance since it has been associated with programmed cell death (*1*). C-type cytochromes are also often part of larger redox enzymes where they work as electron entry/exit points and may even take part in catalytic processes. In addition, heme *c* containing protein domains are frequently found fused to other domains, such as in the $caa_3$ oxygen reductases (*2*).

In cytochromes *c*, the heme prosthetic group is covalently attached to the protein via two thioether bonds to cysteine residues. These amino acids occur in the primary structure, in the large majority of the cases in a CXXCH motif where the histidine residue is one of the axial ligands of the heme iron. In this type of cytochrome, the other axial position may be vacant or occupied by another amino acid residue, such as histidyl or methionyl, the most frequent ones, or in some cases cysteinyl or lysyl. According to Bertini et al. (*2*), at least six classes of single domain, low-spin C-type cytochromes can be identified in prokaryotes, based on phylogeny, amino acid sequence similarity, and function. These classes include cytochromes $c_2$, $c_5$, and $c_6$, and cytochromes $c_{551}/c_{552}$, $c_{553}$, and $c_{552}/c_{554}$, all fitting in the formerly proposed Ambler's class I of cytochromes *c* (*3*).

Several three-dimensional structures of class I cytochromes *c* of different origins have been determined, and they usually show a common conserved fold consisting of at least three α-helices arranged around the heme. Beyond this common fold, the structures of the cytochromes *c* of the different classes are characterized by the presence of further structural elements, such as helices and loops (*4*).

Here we report on the isolation and biochemical and structural characterization of the monoheme cytochrome *c* from *Rhodothermus marinus* (of which several strains have been isolated (*5*), namely, PRQ-62B and ITI 378). This bacterium is Gram-negative, strictly aerobic, and thermohalophilic and belongs to the phylum Bacteroidetes, which consists of three classes: Bacteroidetes, Flavobacteria and Sphingobacteria, *R. marinus* being classified in this last class (*6*). Based on amino acid sequence and structural comparisons, it is proposed that the *R. marinus* cytochrome *c* is the first characterized member of a new class of monoheme C-type cytochromes.

[†] This work was supported by Fundação para a Ciência e a Tecnologia (Grant POCTI/BIA-PRO/58608/2004 to M.T., Grant PTDC/BIA-PRO/66833/2006 to M.A., Grant REEQ/336/BIO/05, and Grant BPD/24193/2005 to M.S.).

[‡] The *Rmcytc* coordinates and structure factors have been deposited in the Protein Data Bank with the accession code 3CP5.

* Corresponding author. Mailing address: Instituto de Tecnologia Química e Biológica, Universidade Nova de Lisboa (ITQB-UNL), Av. da República (EAN) 2780-157 Oeiras, Portugal. Phone: (+351) 214469762. Fax: (+351) 214433644. E-mail: archer@itqb.unl.pt.

[§] Instituto de Tecnologia Química e Biológica, Universidade Nova de Lisboa.

[⊥] Contributed equally to the work.

[||] Faculdade de Engenharia e Ciências Naturais, Universidade Lusófona de Humanidades e Tecnologias.

[¶] Present address: Eco-Bio, Instituto de Investigação Científica Tropical.

[▽] Prokaria Ltd. and University of Iceland.

10.1021/bi800999g CCC: $40.75 
Published on Web 10/15/2008

## EXPERIMENTAL PROCEDURES

*Bacterial Strains, Growth Conditions, and DNA Manipulation.* Liquid cultures of *R. marinus* strains PRQ-62B and ITI 378, two very closely related strains, were grown at 65 °C, in the medium described by Degryse (*7*) with 0.25% yeast extract, 0.25% tryptone, and 1% NaCl added. The *Escherichia coli* XL2-Blue (Stratagene) and BL21-Gold-(DE3) (Stratagene) strains were grown in LB medium supplemented with the appropriate antibiotic.

The DNA region encoding the mature form of cytochrome *c* was amplified from the genomic DNA of *R. marinus* ITI 378 by means of polymerase chain reaction catalyzed by the DNA polymerase *Pfu* Turbo (Invitrogene) and using 5′-GCGGCGC**CCATGG**AAAGC and 5′-GGTTTGTTG**GAATTC**GGCGGAAGTC, as forward and reverse oligonucleotides, respectively.

The blunt end DNA fragment obtained was cloned into pBluescript (Stratagene) previously digested with *Eco*RV (New England Biolabs), and the recombinant plasmid was introduced into *E. coli* XL2-Blue. The cloned DNA was sequenced to confirm the absence of errors upon amplification and cloned into pET22b (Invitrogen) previously restricted with *Nco*I and *Eco*RI (New England Biolabs). *E. coli* BL21-Gold(DE3) carrying the cytochrome *c* maturation genes in the pEC86 vector was used to produce the cytochrome *c* (*8*). To this end, the cell culture was grown in LB medium to an optical density of 0.6 at 600 nm (path length 1 cm), at which point the expression of the cytochrome *c* was induced with 0.1 mM isopropyl-$\beta$-D-thiogalactopyranoside in the presence of 0.8 mg/mL iron sulfate for 4 h at 37 °C in a 30 L reactor, yielding 1.7 g/L of *E. coli* cells (wet weight).

*Purification and Biochemical Characterization of Native and Recombinant R. marinus Cytochrome c.* The native *R. marinus* cytochrome *c* (*Rm*cyt*c*)[1] could not be isolated from the soluble fraction of *R. marinus* PRQ-62B, even after exhaustive washings of the membranes, which may indicate a tight association with another protein in the *R marinus* membranes. It was therefore isolated from solubilized membranes of *R. marinus* PRQ-62B prepared as reported in ref *9*, upon several chromatographic steps.

The solubilized membranes were introduced in a Fast Flow Q-sepharose column equilibrated with 20 mM Tris-HCl, pH 8, and 0.1% dodecyl-$\beta$-D-maltoside (DDM) and eluted in a linear gradient of 0−50% 1 M NaCl. The fraction containing *Rm*cyt*c* was then applied to a chelating Sepharose Fast Flow column saturated with $Ni^{2+}$ and equilibrated with 20 mM Tris-HCl, pH 8, and 0.1% DDM. The *Rm*cyt*c* was eluted in a linear gradient of 0−10% 125 mM imidazole. Complete purification of the protein was only achieved after passing twice on a mono-Q column equilibrated with 2.5 mM Tris-HCl, pH 8, and 0.1% DDM, in which the *Rm*cyt*c* was eluted with a linear gradient of 0−30% 1 M NaCl. After detergent removal by consecutive dilution−concentration steps, the cytochrome *c* was found to be stable in the absence of detergent, suggesting that it is a soluble protein.

The N-terminal amino acid sequence of the native cytochrome *c* was obtained after Edman degradation (*10*), using an Applied Biosystem model 491HT sequencer.

*E. coli* cells expressing the recombinant *Rm*cyt*c* from *R. marinus* ITI 378 were resuspended in 20 mM Tris-HCl, pH 7.5, buffer (buffer A) and broken in a French press at 6000 PSI; cell debris were removed by a 15-min centrifugation at 20 000 × *g*. After separation of soluble and membrane fractions by ultracentrifugation at 138 000 × *g* for 2 h, the soluble fraction was dialyzed in buffer A, concentrated, and applied onto a Q-Sepharose column previously equilibrated in buffer A, and a 0−1 M NaCl gradient was applied. The cytochrome *c* was eluted at 80 mM NaCl. This fraction was concentrated and further applied onto a gel filtration G-50 column equilibrated with buffer A with 150 mM NaCl added. All chromatographic steps were performed in a Pharmacia HiLoad system at 4 °C, and after each purification step, visible spectra and sodium dodecyl sulfate−polyacrylamide gel electrophoresis (SDS-PAGE) analysis were performed. The protein was shown to be pure by SDS-PAGE with a ratio of absorbance 414/280 nm of 5. Since a much higher yield of the overexpressed cytochrome was obtained compared with the native one from strain PRQ-62B, most of the data here reported concern the recombinant protein, which will be called *Rm*cyt*c*. Only when necessary, the mother strain will be specified.

Oxygen consumption by the *R. marinus* PRQ-62B $caa_3$ oxygen reductase was assayed polarographically in a reaction buffer containing 2 mM Tris-HCl, pH 7.5, 0.05% DDM, and 10 mM sodium ascorbate at 50 °C. Fifteen micromolar of either cytochrome and 28 nM of *R. marinus* $caa_3$ oxygen reductase (*11*) were used in the assay. The reaction was inhibited by the addition of 30 $\mu$M KCN. Similarly, the same process was also measured spectrophotometrically in 2 mM Tris/HCl, pH 7.5, and 0.05% DDM, using 2.5 $\mu$M of cytochrome *c* and 0.05 $\mu$M of $caa_3$ oxygen reductase, and the activity was inhibited by KCN, as before.

Amino acid sequence comparisons were performed using Blast at NCBI (*12*), using the Comprehensive Microbial Resource (*13*) databases. Multiple sequence alignments and dendrograms were produced using Clustal X (*14*).

*Spectroscopic Methods.* EPR spectra were measured in a Bruker EMX spectrometer equipped with an ESR900 Oxford Instruments continuous flow helium cryostat at 9.39 MHz microwave frequency, 2.4 mW microwave power, and 10 K. UV−visible absorption spectroscopy on the protein solution was performed in a Shimadzu UV-1603 spectrophotometer, and that on protein crystals using an XSPECTRA microspectrophotometer (4DX-ray Systems AB), both at room temperature. Anaerobic potentiometric titrations were monitored by visible spectroscopy at 25 °C in 50 mM Bis-Tris-Propane, pH 7, using 3.6 $\mu$M of native or recombinant *Rm*cyt*c* in the presence of 15 $\mu$M mediators that cover a range of 0−430 mV (potassium ferricyanide, *N*,*N*-dimethyl-*p*-phenylenediamine, *p*-benzoquinone, 1,2-naphtoquinone 4-sulfonic acid, 1,2-naphtoquinone trimethyhydroquinone, phenazine methosulfate, 1,4-naphtoquinone, duroquinone, and menadione). A silver/silver chloride electrode was used, calibrated against a quinhydrone saturated solution at pH 7.0. The reduction potentials are quoted in relation to the standard hydrogen electrode. The *Rm*cyt*c* reduction was followed at

[1] Abbreviations: *Rm*cyt*c*, *Rhodothermus marinus* cytochrome *c*; DDM, dodecyl-$\beta$-D-maltoside; SDS-PAGE, sodium dodecyl sulfate-polyacrylamide gel electrophoresis; CD, circular dichroism; GuHCl, guanidium hydrochloride; $T_m$, midpoint temperature transition; $T_m^{app}$, apparent midpoint temperature transition; ESRF, European Synchrotron Radiation Facility; PFCC, pseudo-free correlation coefficient.

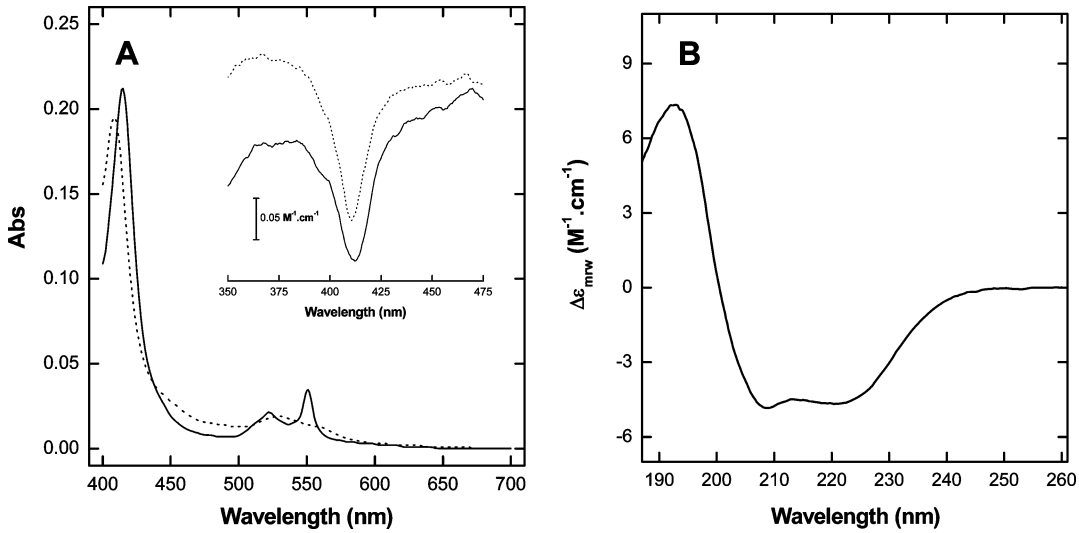


FIGURE 1: (A) Visible and CD−visible absorption (inset) spectra of the reduced (solid line) and oxidized (dotted line) forms of *R. marinus* cytochrome *c* and (B) far-UV CD spectrum of the reduced *R. marinus* cytochrome *c*.

415 nm, and the data points were fitted by a single-electron Nernst curve.

Circular dichroism (CD) spectra of *Rm*cyt*c* (0.1 mg·mL$^{-1}$) were recorded at 25 °C in the far-UV (185−260 nm) and in the visible (340−500 nm) region in quartz cuvettes of 1 mm and 1 cm path lengths, respectively, using a Jasco J-815 CD spectrometer.

*Thermal Stability.* The thermal stability of oxidized *Rm*cyt*c* was investigated by CD spectroscopy. The complete oxidation of the cytochrome was achieved by the addition of 70 $\mu$M potassium hexachloroiridate. Changes in the secondary structure were monitored at 222 nm as a function of temperature from 30 to 95 °C at a heating rate of 1 °C·min$^{-1}$ in the presence of increasing concentrations of the chemical denaturing agent guanidium hydrochloride (GuHCl), using concentrations below the $[GuHCl]_{50\%}$. Thermal unfolding was found to be irreversible, and therefore the thermal unfolding transitions are denoted as apparent to indicate this fact. The thermal unfolding curves, showing distinct pre- and post-transition regions, were analyzed to determine the apparent midpoint temperature transition ($T_m^{app}$) values for the unfolding transition. The obtained $T_m^{app}$ values were plotted as a function of the GuHCl concentration present in each assay and used to extrapolate the $T_m^{app}$ of *Rm*cyt*c*.

*Crystallization and X-ray Diffraction Data Collection of the Rmcytc.* Crystals of recombinant *Rm*cyt*c* were grown at 20 °C using 30% (w/v) poly(ethylene glycol) 8000, 0.2 M ammonium sulfate, 8% (w/v) hexanediol, and 50 mM sodium citrate, pH 2.2, with a protein solution concentrated to 10 mg/mL in 20 mM Tris-HCl buffer, pH 7.5, and 0−0.1 M NaCl. X-ray diffraction data were collected from a single crystal to 1.23 Å resolution on beamline ID14-1 at the European Synchrotron Radiation Facility (ESRF, Grenoble). Crystals belong to monoclinic space group $P2_1$, with unit cell parameters $a = 39.59$, $b = 32.64$, and $c = 42.06$ Å and $\beta = 94.55°$. The asymmetric unit contains one molecule with a molecular mass of 13.8 kDa resulting in an apparent $V_m$ of 1.96 Å$^3$ Da$^{-1}$ and a solvent content of about 37%. More details on crystallization, data collection, and processing statistics are described in ref *15*.

*Structure Determination and Refinement.* Intensity data were transformed to structure factor amplitudes with the

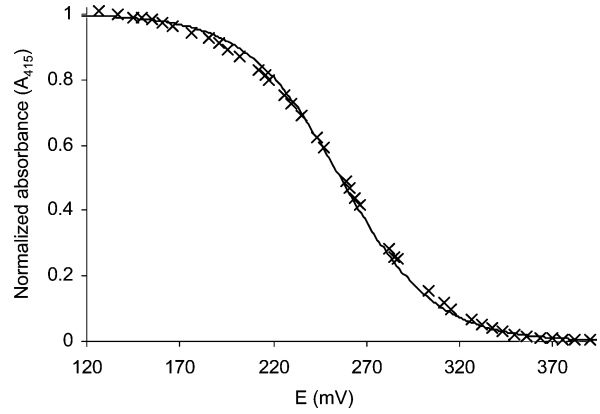


FIGURE 2: Redox titration of *R. marinus* cytochrome *c* (theoretical curve = solid line, experimental points = crosses). The solid line was calculated from a single-electron Nernst curve with $E° = 260$ mV.

program TRUNCATE from the CCP4 program suite (*16*). The structure of *Rm*cyt*c* was solved by the SAD method using the anomalous scattering of the heme iron, despite the relatively low anomalous signal of the iron atom at the wavelength of 0.934 Å ($f'' = 1.37$ e$^-$), which leads to an overall Bijvoet ratio of $|\Delta F^{\pm}|/|F|$ of 0.92%. The position of the heme-iron atom was determined with SHELXD (*17*) after analyzing the structure factors using SHELXC (*18*). Phase calculation and density modification were then performed with the program SHELXE (*19*). First phasing trials assuming a solvent content of 37% and applying 20 cycles of density modification did not lead to an interpretable electron density map. However, by increasing the number of cycles of density modification to 55, the phase refinement converged with a pseudo-free correlation coefficient (PFCC) of around 80%. Further improvement of the phases was achieved using the "free lunch algorithm" (*20*) implemented in SHELXE, which allows extrapolation of the data beyond the experimentally measured resolution. Final phases obtained by extrapolating the data resolution to 0.8 Å were characterized by a PFCC of 82.8% and led to a very well defined experimental electron density map that enabled automated model building with ARP/WARP (*21*) of 92 out of 124 residues. The partial model including the heme group was

Table 1: Data Collection, Processing, and Refinement Statistics

| | |
|---|---|
| wavelength (Å) | 0.934 |
| resolution range (Å) | 42.41 (1.30−1.23)[a] |
| $R_{merge}$ | 0.084 (0.480)[a] |
| $R_{p.i.m.}$ | 0.023 (0.338)[a] |
| number of observed reflections | 276576 (9595)[a] |
| number of unique reflections | 29745 (3380)[a] |
| mean ($I/\sigma(I)$) | 13.6 (1.6)[a] |
| completeness (%) | 96.3 (75.9)[a] |
| multiplicity | 9.3 (2.8)[a] |
| resolution range for refinement (Å) | 10.0−1.23 (1.30−1.23)[a] |
| number of unique reflections in refinement | 29669 |
| working set | 28180 |
| test set | 1489 |
| completeness (%) | 96.4 (73.3)[a] |
| R-factor (%) ($F > 4\sigma(F)$) | 13.0 (10.7) |
| free R-factor (%) ($F > 4\sigma(F)$) | 17.4 (15.0) |
| number of non-hydrogen atoms | 1183 |
| number of protein atoms[b] | 951 |
| number of heterogen atoms[b] | 48 |
| number of solvent atoms[b] | 168 |
| Weighted rms Deviations from Ideal Values | |
| bond length (Å) | 0.015 |
| angle distances (Å) | 0.033 |
| angles (deg) | 1.89 |
| B wilson (Å$^2$) | 8.6 |
| average B-factor (Å$^2$) | |
| main chain/side chain | 12.7/18.8 |
| all non-H protein atoms | 15.8 |
| water molecules | 29.2 |
| heme group | 8.9 |
| sulfate ion | 28.8 |

[a] Values in parentheses refer to the indicated resolution shell. [b] Non-hydrogen atoms.

completed manually using COOT (*22*) alternated with structure refinement using SHELXL (*23*). Five percent of randomly selected reflections were used for cross-validation. After initial 20 cycles of isotropic refinement, anisotropic atomic displacement parameters were refined. Inspection of the $\sigma_A$ electron density maps (*24*) allowed addition of water molecules and a sulfate ion and building of alternate conformations for some side chains. The final 10 refinement cycles included hydrogen atoms on riding positions. Standard restraints were applied to the geometrical (*25*) and isotropic or anisotropic displacement parameters (*23*), except for the heme and sulfate groups. The final values of R-factor and R-free converged to 13.0% and 17.4%, respectively.

*Structure Analysis and Comparison with Other C-type Cytochromes.* Secondary structure assignments and solvent-accessible surfaces were calculated with the programs DSSP (*26*) and Whatif accessibility program (*27*), respectively. Secondary structure matching was carried out using the protein structure comparison service SSM at the European Bioinformatics Institute (*28*). A structure-based multiple sequence alignment among 3D structures of different C-type cytochromes was generated using SSM. The alignment was then used to generate a dendrogram using the neighbor joining method (*29*) implemented in CLUSTALW (*14*), which was plotted using the program DRAWTREE from the PHYLIP package (*30*).

## RESULTS AND DISCUSSION

*Production and Biochemical Characterization of Rmcytc.* A monoheme cytochrome *c* was purified from the membranes of *R. marinus* PRQ-62B. The N-terminal sequence of this cytochrome (TESGTGTQDPETLAAEIGPVKQ) allowed the identification of its encoding gene in the *R. marinus* ITI 378 partial genome library (deposited at GenBank EU361735); the N-terminal sequence is 86% identical to the *R. marinus* ITI 378 orthologue. The analysis of the genomic organization revealed that the gene coding for the *Rm*cyt*c* is flanked upstream by a gene encoding a putative transcriptional regulator and downstream by a gene coding for a putative nitrous oxide reductase. The whole cytochrome *c* open reading frame comprises 492 base pairs, encoding a 163-amino acid precursor polypeptide. The mature cytochrome lacks the first 39 amino acid residues, which constitute a periplasmic signal peptide of the Sec type, as is typical for C-type cytochromes, which are exported as apoproteins into the periplasm, where the insertion of the heme group occurs (*31, 32*). The next 124 amino acid residues constitute the mature form of the *Rm*cyt*c*, whose molecular mass is 13.8 kDa.

Since the wild-type cytochrome could only be isolated in small amounts from the membranes of *R. marinus* PRQ-62B, *R. marinus* ITI 378 cytochrome *c* was overexpressed in *E. coli* (*Rm*cyt*c*) in the presence of the cytochrome *c* maturation genes (*8*) to allow further biochemical and structural characterization. The recombinant *Rm*cyt*c* was purified from the soluble fraction, and thoroughly characterized to confirm its integrity for subsequent studies, such as thermostability and X-ray structure.

The apparent molecular mass of the wild-type and recombinant proteins, determined by SDS-PAGE, was 14 kDa, in agreement with the predicted value (data not shown). The cytochromes were purified in the reduced form, having identical visible spectra with maxima of the Soret and α bands at 415 and 550 nm, respectively. Upon oxidation with ammonium persulfate, the maximum of the Soret band shifts to 408.5 nm (Figure 1A). The protein crystallized in the oxidized form, as revealed by microspectrophotometry of the crystals. The EPR spectrum of the oxidized cytochromes presented a $g_{max}$ value of 3.28 (data not shown), which indicates a quasi-axial ligand field at the heme iron. The visible CD spectra of the reduced recombinant cytochrome *c* showed a trough near 408 nm, typical of heme-containing proteins (*33*); the spectrum of the oxidized protein is slightly red-shifted (Figure 1A, inset). In addition, the far-UV CD spectrum of the as purified protein is typical of a folded α-helical protein, with the characteristic negative band with two peaks at 208 and 222 nm and a positive band at 193 nm (Figure 1B) (*34*).

A redox titration followed by visible absorption spectroscopy was performed at pH 7 and revealed a reduction potential of +260 ± 10 mV (Figure 2), for both native and recombinant *Rm*cyt*c*. This reduction potential is within the range reported for other bacterial C-type cytochromes (see ref *35* for review).

C-type cytochromes are involved in the aerobic electron transport chains of most aerobic organisms; therefore, functional studies were performed to determine whether these cytochromes exchange electrons with the $caa_3$ oxygen reductase, one of the oxidases that compose the aerobic respiratory chain of *R. marinus* (*36*). The reduced cytochromes were completely oxidized upon addition of $caa_3$; the subsequent addition of potassium cyanide, a heme−copper oxygen reductase inhibitor, led to re-reduction of the

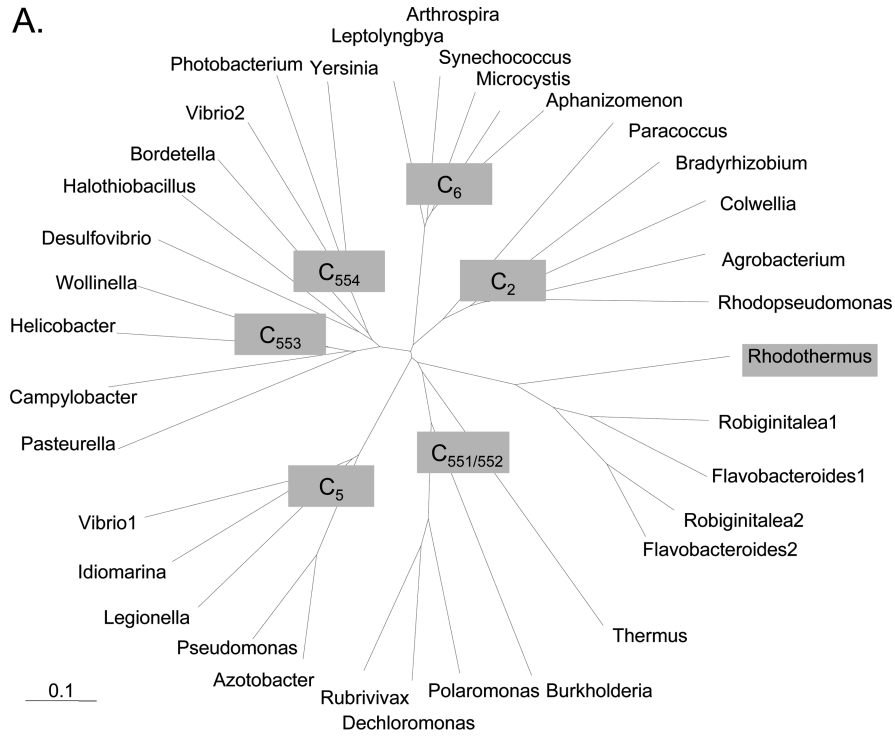


B.

| | | Rm_Cytc | | $C_2$ | | $C_5$ | | $C_6$ | | $C_{551/552}$ | | $C_{553}$ | | $C_{554}$ | |
|---|---|---|---|---|---|---|---|---|---|---|---|---|---|---|---|
| | | m | M | m | M | m | M | m | M | m | M | m | M | m | M |
| Rm_Cytc_like | I | 35 | 41 | | | | | | | | | | | | |
| | S | 59 | 61 | | | | | | | | | | | | |
| $C_2$ | I | 8 | 12 | 18 | 42 | | | | | | | | | | |
| | S | 19 | 24 | 32 | 62 | | | | | | | | | | |
| $C_5$ | I | 11 | 12 | | | 30 | 68 | | | | | | | | |
| | S | 17 | 23 | | | 45 | 84 | | | | | | | | |
| $C_6$ | I | 8 | 14 | | | | | 48 | 63 | | | | | | |
| | S | 21 | 23 | | | | | 62 | 73 | | | | | | |
| $C_{551/552}$ | I | 7 | 10 | | | | | | | 3 | 53 | | | | |
| | S | 17 | 23 | | | | | | | 11 | 67 | | | | |
| $C_{553}$ | I | 10 | 13 | | | | | | | | | 23 | 45 | | |
| | S | 22 | 28 | | | | | | | | | 39 | 66 | | |
| $C_{554}$ | I | 8 | 13 | | | | | | | | | | | 21 | 45 |
| | S | 19 | 24 | | | | | | | | | | | 32 | 61 |

FIGURE 3: Amino acid sequence comparison of *R. marinus* ITI 378 cytochrome *c* with prokaryotic C-type monoheme cytochromes: (A) dendrogram; (B) table with Maximal (M) and minimal (m) identity (I) and similarity (S) percentage among cytochrome *c* sequences from different groups (accession numbers in parentheses). *Agrobacterium*, *A. tumefaciens* (P00081); *Aphanizomenon*, *A. flos-aquae* (P00116); *Arthrospira*, *A. maxima* (P00118); *Azotobacter*, *A. vinelandii* (AAC45922); *Bordetella*, *B. pertussis* (NP_881117); *Bradyrhizobium*, *B. japonicum* (BAC47653); *Burkholderia*, *B. dolosa* (ZP_00982883); *Campylobacter*, *C. jejuni* (NP_282300); *Colwellia*, *C. psychrerythraea* (YP_270114), *Dechloromonas*, *D. aromatica* (AAZ45778); *Desulfovibrio*: *D. vulgaris* (YP_012252); Flavobacteroides1, *F. bacterium* (ZP_01105921); Flavobacteroides2, *F. bacterium* (ZP_01105294); *Halothiobacillus*, *H. neapolitanus* (P25938); *Helicobacter*, *H. pylori* (NP_20801); *Idiomarina*, *I. baltica* (ZP_01041945); *Legionella*, *L. pneumophila* (YP_096733); *Leptolyngbya*, *L. boryana* (P00117); *Microcystis*, *M. aeruginosa* (P00112); *Paracoccus*, *P. denitrificans* (C2P00096); *Pasteurella*, *P. multocida* (NC_002663), *Photobacterium*, *Photobacterium* sp. (ZP_01162384); *Polaromonas*, *P. naphthalenivorans* (ZP_01020507); *Pseudomonas*, *P. fluorescens* (YP_351250); *Rhodothermus*, *R. marinus* (EU361735); *Rhodopseudomonas*, *R. viridis* (1co6); *Robiginitalea*1, *R. biformata* (ZP_01120248); *Robiginitalea*2, *R. biformata* (ZP_01119795), *Rubrivivax*, *R. gelatinosus* (ZP_00243317), *Synechococcus*, *Synechococcus* sp. (P00115); *Thermus*, *T. thermophilus* (1c52); *Vibrio*1, *V. cholerae* (NP_229825), *Vibrio*2, *V. cholerae* (NP_231872); *Wolinella*, *W. succinogenes* (NP_906926); *Yersinia*, *Y. pestis* (CAC89905).

cytochrome, due to its "autoreducible" properties. In addition, a cytochrome *c*/oxygen oxidoreductase activity of 9 $min^{-1}$, determined polarographically, was 100% inhibited by KCN. The ability of *Rm*cyt*c* to reduce *Rmcaa*$_3$ suggests that it may function as part of the aerobic respiratory chain of this bacterium. However, this activity is significantly lower than the oxidation by the *caa*$_3$ oxygen reductase of the high-potential iron−sulfur protein, an electron carrier also present in the organism (*11*), and, in fact, so low that class I cytochromes from any source could be expected to give a similar level of activity. Thus no conclusion can be made about the physiological relevance of this reaction. This suggests that cytochrome *c* may be the preferred electron donor to another oxygen reductase of *R. marinus* respiratory chain, namely, the *cbb*$_3$ (*37*) or *ba*$_3$ (*38*) oxygen reductases. In accordance with this, in the aerobic respiratory chain of *Thermus thermophilus*, which also contains a *caa*$_3$ enzyme, the cytochrome $c_{552}$ is the physiological redox partner of the *ba*$_3$ oxygen reductase (*39*).

*Amino Acid Sequence Comparisons.* The amino acid sequence of the *Rm*cyt*c* was used to search the NCBI data bank for homologous proteins. The most similar hits

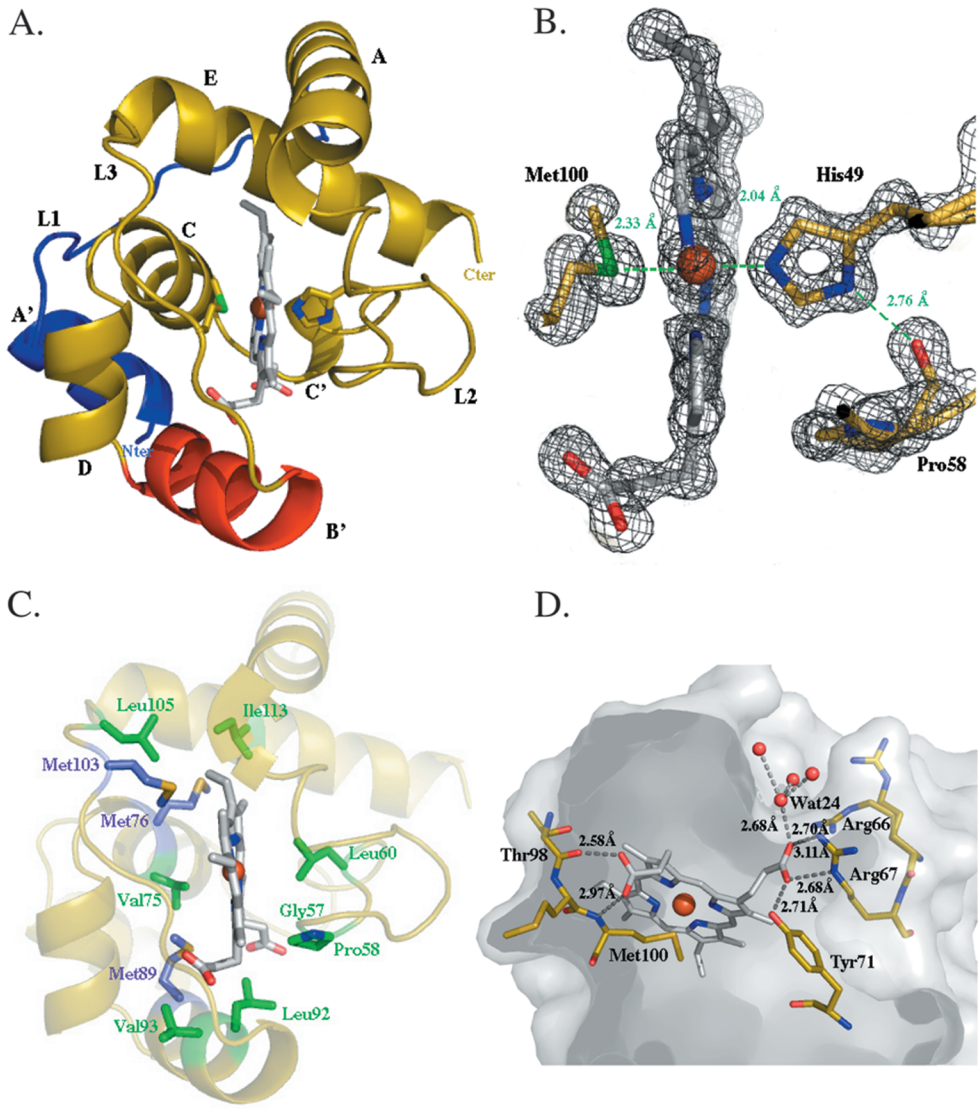


FIGURE 4: (A) *Rm*cyt*c* overall structure in cartoon representation. The heme and the axial iron ligands His49 and Met100 are shown in stick representation. The uncommon N-terminal helix (A′) and loop are shown in blue and the uncommon inserted helix (B′) in red. The view corresponds to the standard front orientation with the exposed edge of the heme toward the viewer with the histidine residue Fe ligand to the right. (B) Close-up view of the heme and the axial ligands, and the hydrogen bond accepting carbonyl oxygen atom of Pro58. The refined $\sigma_A$ electron density map of the residues is shown, contoured at $2\sigma$. (C) Hydrophobic heme environment of *Rmcytc*. Hydrophobic residues (green) with side chain atoms within 4 Å of the heme (gray) are shown in stick representation; methionines are in violet. (D) Possible interactions of the heme propionate groups with neighboring protein residues. The carbon atoms of the heme are shown in gray, and those of the peptide backbone are in yellow. Water molecules are shown as red spheres, and the protein surface is indicated in gray. On the left, the D ("outer") propionate points toward the lower front part of the protein; on the right, the A ("inner") propionate points toward the lower back of the protein and is in contact with the solvent via Wat24. The side chain of Arg66 occupies two alternate conformations, one with the NH2 atom within hydrogen bonding distance of the heme propionate and the other with the side chain pointing toward the solvent.

represent proteins that contain motifs to bind a heme C from bacteria belonging to the Phylum Bacteroidetes, in which *R. marinus* is included. To date, there are no reports on the biochemical or structural characterization of those proteins. The *Rm*cyt*c* primary structure was compared with the best hits resulting from the data bank search and other monoheme C-type cytochromes from different classes, all matching the criteria for Ambler's class I, namely, cytochromes $c_2$, $c_5$, $c_6$, $c_{551/552}$, $c_{553}$, and $c_{554}$ (see ref *2* for a review), producing the dendrogram shown in Figure 3A. It was possible to identify a group formed by the *R. marinus*-like cytochromes *c*, which is not included in any of the pre-existing classes of monoheme C-type cytochromes (Figure 3). Corroborating the data from the dendrogram, the percentage of identity and similarity between the proteins in the *R. marinus*-like cytochromes *c* group is clearly higher among each other than compared with cytochromes *c* from the other groups analyzed (Figure 3B), thus suggesting that *Rm*cyt*c* is the first studied member of a new class of C-type cytochromes. Further structural evidence emphasizes this proposal (see below).

*X-ray Structure and Model Quality.* The crystal structure of *Rm*cyt*c* was determined by the SAD method using the anomalous scattering of the heme iron at 0.934 Å and refined to 1.23 Å resolution with an R-factor of 13.0% (R-free of 17.4%). The final model contains 116 residues (Asp9 to Gln124), the heme group, 168 water molecules, of which 101 are fully occupied and 67 were modeled with half-occupancy, and 1 sulfate ion. This sulfate ion mediates a crystal contact between neighboring protein molecules

A.

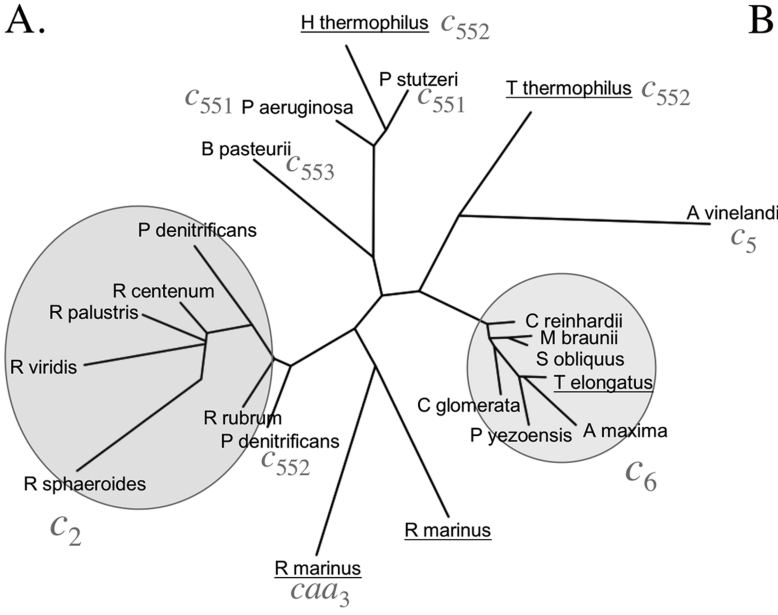


B.

| Organism | Pdb-code | RMSD[a] [Å] | Q[b] | % seq[c] | nbr residues[d] |
|---|---|---|---|---|---|
| *Rhodothermus marinus* | - | | | | 116 |
| **Cytochrome *c*6** | | | | | |
| *Monoraphidium braunii* | 1ctj | 2.0 | 0.35 | 19 | 89 |
| *Chlamydomonas reinhardii* | 1cyj | 2.0 | 0.33 | 29 | 90 |
| *Thermosynechococcus elongatus* | 1c6s | 2.4 | 0.31 | 21 | 87 |
| *Arthrospira maxima* | 1f1f | 2.4 | 0.33 | 22 | 88 |
| *Scenedesmus obliquus* | 1c6r | 2.1 | 0.33 | 23 | 88 |
| *Porphyra yezoensis* | 1gdv | 2.3 | 0.36 | 25 | 85 |
| *Cladophora glomerata* | 1ls9 | 2.1 | 0.35 | 26 | 91 |
| **Cytochrome *c*553** | | | | | |
| *Bacillus pasteurii* | 1b7v | 1.7 | 0.38 | 22 | 71 |
| **Cytochrome *c*552** | | | | | |
| *Thermus thermophilus* | 1c52 | 1.8 | 0.23 | 22 | 131 |
| *Pseudomonas nautica* | 1cno:D | 2.2 | 0.29 | 21 | 86 |
| *Paracoccus denitrificans* | 1ql3:A | 1.3 | 0.40 | 27 | 99 |
| *Hydrogenobacter thermophilus* | 1ayg | 2.0 | 0.32 | 22 | 80 |
| *Hydrogenophilus thermoluteolus* | 2d0s | 1.9 | 0.35 | 22 | 79 |
| **Cytochrome *c*2** | | | | | |
| *Rhodospirillum rubrum* | 3c2c | 1.6 | 0.31 | 24 | 112 |
| *Rhodobacter capsulatus* | 1c2r:A | 2.4 | 0.21 | 21 | 116 |
| *Rhodobacter sphaeroides* | 1cxc | 3.1 | 0.20 | 10 | 124 |
| *Rhodopseudomonas viridis* | 1co6 | 1.6 | 0.32 | 24 | 107 |
| *Rhodopseudomonas palustris* | 1fj0:B | 2.5 | 0.23 | 24 | 114 |
| *Paracoccus denitrificans* | 1cot | 1.5 | 0.30 | 26 | 121 |
| *Rhodospirillum centenum* | 1jdl | 2.6 | 0.20 | 22 | 118 |
| **Cytochrome *c*5** | | | | | |
| *Azotobacter vinelandii* | 1cc5 | 2.4 | 0.23 | 23 | 83 |
| **Cytochrome *c*551** | | | | | |
| *Pseudomonas stutzeri* | 1fi3 | 1.9 | 0.37 | 29 | 82 |
| *Pseudomonas aeruginosa* | 451c | 1.8 | 0.36 | 26 | 82 |
| *Paracoccus denitrificans* | 2mta:C | 2.0 | 0.28 | 19 | 147 |
| *Ectothiorhodospira halophila* | 1gks | 2.2 | 0.27 | 18 | 78 |

FIGURE 5: (A) Monohemic cytochrome *c* dendrogram. The dendrogram illustrates structural relationships among the different molecules. It was generated from the secondary structure based multiple sequence alignment using the neighbor joining method (*29*). (B) Comparison of bacterial single domain monoheme cytochromes *c* of the different families by pairwise secondary structure matching using SSM (*28*). Thermophilic organisms are underlined. [a]Root mean square deviation between Cα-atoms of matched residues at best 3D superposition of the query structures by pairwise secondary structure matching using SSM (*28*). [b]Quality of alignment: $Q = (N_{algn}N_{algn})/((1 + (RMSD/R_0)^2)N_{res1}N_{res2})$ takes into account both the alignment length ($N_{algn}$) and RMSD. $N_{res1}$ and $N_{res2}$ are the number of residues in the aligned proteins; $R_0$ is an empirical parameter, set to 3 Å. [c]Fraction of pairs of identical residues among all aligned. [d]Number of residues in pdb file. Gray shaded fields correspond to thermophilic organisms.

involving a hydrogen bond with a protonated carboxylate oxygen of Glu122. The electron density maps are generally very well defined, except for residues Gly26, Glu27, and the C-terminal Gln124 and the side chains of surface residues Arg66, Asn80, and Arg85. The first eight residues are not visible in the maps. Alternate conformations were modeled for nine residues, namely, Leu13, Ser24, Asn42, Thr46, Met73, Arg85, Thr101, and Ser106. All non-glycine residues lie in most favored (95%) or additionally allowed (4%) regions of the Ramachandran plot (*40*), except for Phe55, whose conformation is stabilized by a cation−$\pi$ interaction with Arg50 and its $2F_o - F_c$ density map is well-defined. Statistics on data collection and processing, and relevant parameters of refinement are presented in Table 1.

*Overall Fold and Heme Moiety.* The X-ray structure of *Rm*cyt*c* comprises seven α-helices connected by random coil fragments, which are folded around the heme group (Figure 4A). Helices A, C, and E form the typical monoheme cytochrome *c* fold (*4*). These helices, along with helix B′, loops 2 and 3, and the short helix C′, enclose the heme. The helices and loop regions are connected by three bends and two hydrogen-bonded turns. Interestingly, *Rm*cyt*c* has an uncommon N-terminal extension consisting of 21 amino acid residues that forms the α-helix A′ and loop 1, which wrap around the back of the protein. A further unusual structural element of *Rm*cyt*c* is α-helix B′, inserted between helix D and loop 3, that shields the lower part of the heme from solvent (Figure 4A).

Heme *c* is covalently attached to the polypeptide chain by two thioether bonds involving the sulfhydril groups of Cys45 and Cys48. The heme iron is axially coordinated by His49 and Met100. Moreover, the Nδ1 atom of His49 is H-bonded to the carbonyl oxygen of Pro58 (Figure 4B), which should play a role in the correct orientation of the histidyl side chain for iron ligation. Cys45, Cys48, and His49 are part of loop 2, whereas Met100 is located on loop 3. As in many C-type cytochromes (*4, 41*), in *Rm*cyt*c*, the heme is not planar, the pyrrole rings being asymmetrically tilted at angles between 5.7° and 7.6° to the heme "plane" and the porphyrin ring itself being bent with the largest deviation from planarity of about 15° between pyrrole rings B and C that link the heme to the cysteine residues.

The heme group is located in a mostly hydrophobic pocket and is almost completely shielded from the solvent (only 7% of its surface is solvent-accessible). The heme pocket and the hydrophobic residues within 4 Å distance of the heme are depicted in Figure 4C. As usual for this type of cytochrome, the atoms CMC and CBC of the pyrrole ring are solvent-accessible, with accessible surface areas of 3.8 and 11.0 Å$^2$, respectively. In contrast to a number of larger cytochromes *c* ($c_2$, mitochondrial, $c_{552}$), the backward facing propionate A (inner propionate) of the heme is also partly exposed to solvent (depending on the conformation of Arg66, accessible surface area of 0.3−3.3 Å$^2$) and is located in a positively charged area of the heme pocket. The H-bonding established by the heme propionate groups is illustrated in Figure 4D.

*Structural Comparison.* The coordinates of *Rm*cyt*c* were submitted to the Secondary Structure Matching, SSM, server (*28*) to search for similar structures in the Protein Data Bank. The most similar structure is the C-terminal domain of the $caa_3$ oxygen reductase of *R. marinus* (*42*) (27% identity, 51% similarity), followed by several mitochondrial cytochromes *c* and cytochrome $c_{553}$ from *Bacillus pasteurii*. A structural comparison between *Rm*cyt*c* and representatives of the different families of C-type cytochromes was performed. Due to the large number of cytochrome *c* structures available and for the sake of simplicity, we will consider only the bacterial

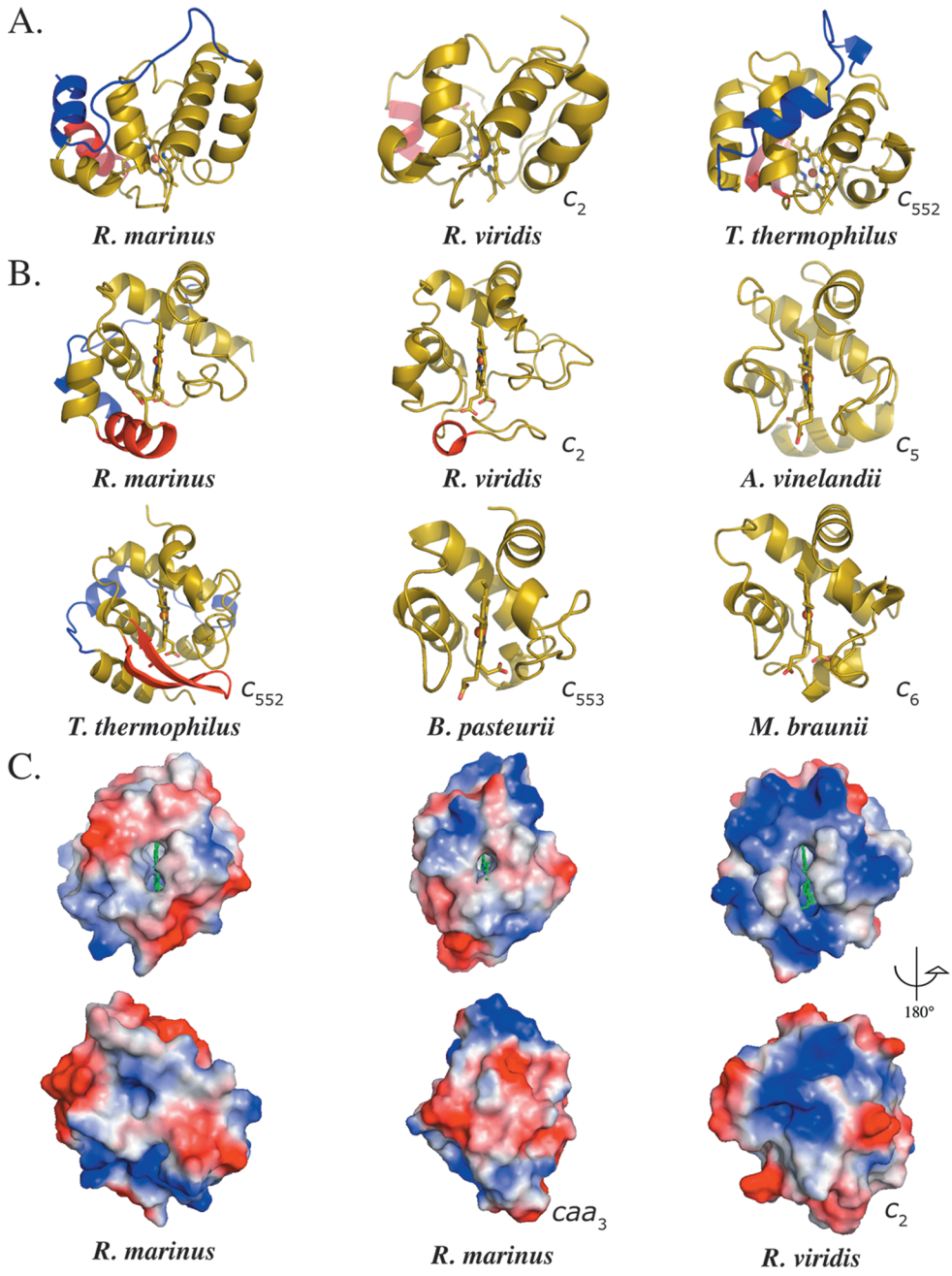


FIGURE 6: (A) Cartoon representation of cytochrome *c* structures. View of the heme distal side of the indicated cytochrome *c* structures. The N-terminal helix A′ and loop 1 in *Rm*cyt*c* and the C-terminal extension in *T. thermophilus* cytochrome $c_{552}$ are in blue. (B) View of the front side of the molecules. Helix B′ in the *Rm*cyt*c* structure and secondary structure elements that occupy similar spatial positions as *Rm*cyt*c* helix B′ in *R. viridis* cytochrome $c_2$ and in *T. thermophilus* $c_{552}$ are shown in red. (C) Electrostatic surface potential maps of the cytochrome *c* structures. The upper row shows the molecules' front view with the exposed edge of the heme toward the viewer, with the histidine Fe ligand to the right. For the lower row, the models were rotated by 180° about the vertical axis. Coloring is made according to the calculated electrostatic potential from negative (red) to positive (blue) values. The electrostatic potential limits are ±61.8, ±51.3, and ±57.8 kT/e for *R. marinus* cytochrome *c*, the heme domain of $caa_3$ oxygen reductase, and *R. viridis* cytochrome $c_2$, respectively. The calculation of the electrostatic potential is based only on the peptide and does not include the heme charges.

monoheme cytochromes throughout this study and not the mitochondrial ones or those inserted in larger complexes, except when this is of particular interest. In order to obtain an overview of the structural families of monoheme cytochromes *c* and to position *Rm*cyt*c* relative to them, a dendrogram of a multiple structure-based sequence alignment was constructed (Figure 5), and the secondary structure matching corroborates the results of the amino acid sequence comparisons (Figure 3). *Rm*cyt*c* presents particular structural features as compared with the cytochrome *c* families characterized so far.

One striking structural feature of *Rm*cyt*c* is the N-terminal extension that consists of helix A′ followed by loop 1, which entwines around the back of the molecule (Figure 4A). So far, such an extension has only been observed in the *T. thermophilus* cytochrome $c_{552}$ structure, but at the C-terminus not at the N-terminus (*43*) (Figure 6A). The other unusual structural element of *Rm*cyt*c* is α-helix B′ located between helix D and loop 3 (Figure 4A). A similar but shorter helix is also present in cytochromes $c_2$ (Figures 6A,B) and in mitochondrial cytochromes *c*, although in a different place of the amino acid sequence. In contrast, no such feature as

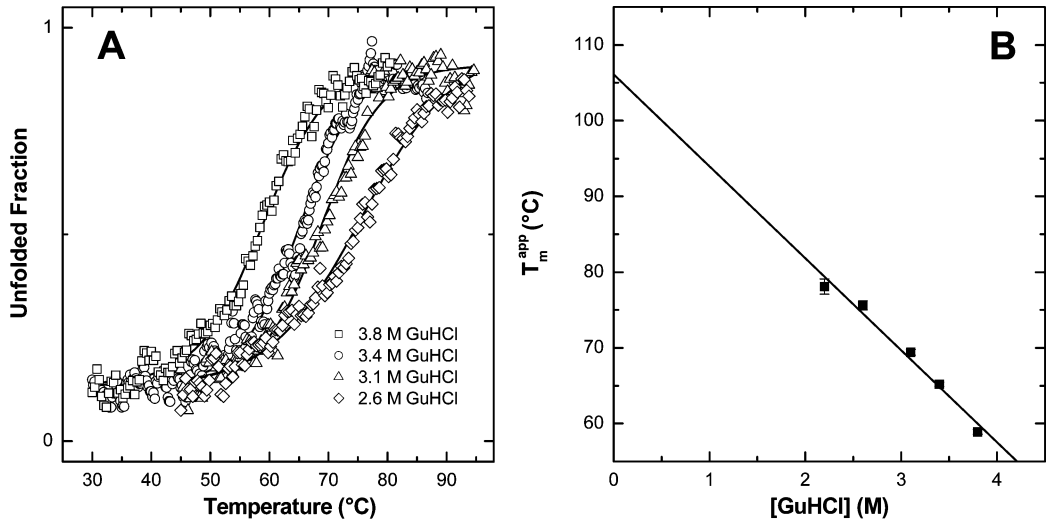


FIGURE 7: (A) Thermal unfolding of oxidized *R. marinus* cytochrome *c*. Thermal denaturation in the presence of 2.6, 3.1, 3.4, and 3.8 M GuHCl. The solid lines correspond to the sigmoidal fitting of the data, from which the $T_m^{app}$ are determined. (B) Determination of the $T_m^{app}$ in water (i.e., [GuHCl] = 0) by linear extrapolation of the midpoint transition temperatures obtained at different GuHCl concentrations.

helix B′ is observed in smaller cytochromes *c*, such as $c_{553}$, $c_5$, or $c_6$. In *T. thermophilus* cytochrome $c_{552}$, there is a two-stranded $\beta$-sheet instead.

These structural motifs occupying similar regions in the proteins but distinct places in the respective amino acid sequences support divergent evolution of C-type cytochromes, with several independent DNA deletion and insertion events. The amino acid residues forming helix B′ and loop 1 of the N-terminal extension of *Rm*cyt*c* are very conserved in the primary structure of the monoheme *Rm*cyt*c*-like cytochromes from bacteria of the Bacteroidetes phylum, suggesting that these motifs may be common structural features of this class of cytochromes. Amino acid sequence comparison with other cytochromes *c* show that the regions corresponding to these structural elements are not present in the cytochromes *c* from organisms other than bacteria of the Bacteroidetes phylum. This, together with the phylogenetic analysis and structural comparison (Figures 3 and 5), corroborates that the bacteroidetes cytochromes *c* form a new subfamily, of which the *R. marinus* cytochrome *c* is the first characterized member.

In contrast to a large number of cytochromes *c* whose crystal structures have been determined, *Rm*cyt*c* structure does not contain any ordered internal water molecule. However, Wat24, which corresponds to Wat125 in horse heart cytochrome *c* (*44*), is H-bonded to the carboxylate group of propionate A and to the highly conserved Arg66 (Figure 4D). In *Rm*cyt*c*, this water molecule is in contact with other ordered solvent molecules and is not buried in the heme cavity, as in mitochondrial cytochrome *c*.

It is worth noting the high overall number of methionines in *Rm*cyt*c* (seven) compared with a usual average of two methionines per cytochrome *c*. All methionines are located between residues 76 and 103, corresponding to a ratio of one methionine per four residues in this interval. Structurally, all these methionines are located on the lower front side of the molecule to the left of the heme. Four of these methionines are in the immediate heme environment, where Met76 replaces the usually invariant leucine or isoleucine (Leu68 in tuna) and Met103 replaces phenylalanine or tyrosine (Phe82 in tuna numbering) (Figure 4C). The high content in methionine residues in this region of the sequence is a conserved feature among the *Rm*cyt*c*-like proteins of the Bacteroidetes phylum. Similar to those in the thermophilic *Thermosynechococcus elongatus* cytochrome $c_6$ (*45*), two of the methionines are flanking the heme crevice.

*Electrostatic Properties.* The front face of *Rm*cyt*c*, as illustrated in Figure 4C, is composed mainly of hydrophobic residues that form the immediate environment of the exposed heme edge, as also observed for the other bacterial and mitochondrial monoheme C-type cytochromes. In *Rm*cyt*c*, these hydrophobic residues are Ala47, Ile56, Phe55, Met99, Met103, and Tyr44. The front face of *Rm*cyt*c* also contains patches of preponderant negative and a few positive electrostatic potential regions. The negative electrostatic potential surface patch centered around Asp102 is in close proximity to the heme edge and is uncommon among the studied cytochromes *c* (Figure 6C).

A large concentration of negative charges on the top and of positive charges on the bottom of *Rm*cyt*c* lead to a dipole moment that is almost parallel to the heme plane and points downward. In contrast, the surface of the basic *Rhodopseudomonas viridis* cytochrome $c_2$ is charged in a different asymmetric manner, its front face (as shown in Figure 6C) being composed of hydrophobic residues and lysines that cluster around these latter residues and on the left and right sides, while the back side of the molecule contains in addition carboxylates (*4*). In bacterial and mitochondrial cytochromes *c*, the surface area on the front side, around the exposed heme edge, has been implicated as the interaction site for other redox proteins (*4, 42*). The direction of the dipole moments might be important for the initial mutual orientation of the redox partners for forming an electron transfer complex. *Rm*cyt*c* can donate electrons to the organism's $caa_3$ reductase. The cytochrome *c* domain of subunit II from the $caa_3$ enzyme, whose structure is known (*42*), is the entry point for electrons in the oxidase, and it has been suggested that its heme C pyrrole edge, surrounded mostly by hydrophobic residues, is exposed to the surface and free to accept electrons from the electron transfer partner. Comparison of the electrostatic surface potential of the front sides of *Rm*cyt*c* and the $caa_3$ cytochrome *c* domain (Figure 6C) suggests that

complex formation between the two molecules may involve the hydrophobic regions around the exposed heme edges, enhanced by complementarily charged surface regions in a similar way as that observed for the yeast $bc_1$/cytochrome *c* complex (*46*). It is also possible that *Rm*cyt*c* establishes contacts with parts of the $caa_3$ oxygen reductase beyond the subunit II C-domain as observed in the cytochrome $c_{552}-ba_3$ oxygen reductase electron transfer complex (*47*).

*Thermostability.* The thermostability of a protein results from versatile stabilization strategies that correspond to subtle structural modifications. For *Rm*cyt*c*, one of the stabilizing factors may be the N-terminal extension, clasping around the back of the molecule. Further parameters have been pointed out to promote protein thermostability, such as a high number of hydrogen bonds between side chains, number of salt bridges, or the presence of certain amino acid residues (*49*). *Rm*cyt*c* contains 12 H-bonds between pairs of side chains, five of which are established by amino acid residues located on the N-terminal helix A′ and residues on adjacent helices C and D, four additional salt bridges, and also eight arginine residues. In *T. thermophilus* cytochrome $c_{552}$, the C-terminal extension that wraps around the back of the molecule in a similar manner to the N-terminal extension in *Rm*cyt*c* (Figure 6A) was suggested to serve as a clamp tied to the remainder of the tertiary structure, thus contributing to the high thermostability of the protein, the extra clamp being tied to the remainder of the structure by a higher-than-average number of ion pairs as well as hydrophobic contacts (*43*). Nevertheless, with the exception of the already mentioned cytochrome $c_{552}$ from *T. thermophilus*, the four 3D structures of single domain monoheme cytochromes *c* from thermophilic organisms that are known (*43, 45, 50, 51*) are not related by any common particularities that would distinguish them from their mesophilic counterparts, exhibiting the typical structural characteristics of their families.

The thermal stability of the oxidized *Rm*cyt*c* was investigated by monitoring the variation of the CD signal at 222 nm, which is indicative of the conformational status of a protein. The as-prepared protein at pH 7 does not unfold up to 100 °C. Therefore, in order to lower the midpoint temperature transition ($T_m$) to a measurable range, temperature-induced denaturation curves were determined in the presence of increasing concentrations (from ~2 to 4 M) of the chemical denaturant agent GuHCl (Figure 7A). The plot of the $T_m^{app}$ at different GuHCl concentrations was used to determine the $T_m^{app}(H_2O)$ in water by linear extrapolation (Figure 7B). The value calculated for *Rm*cyt*c* was 106 ± 3 °C, which is of the same order of magnitude as the $T_m^{app}$ of cytochrome $c_{552}$ from the moderately thermophilic bacteria *Hydrogenobacter thermophilus* (~110 °C) (*52*) and *Pseudomonas hydrogenothermophila* (108 °C) (*51*), also determined in the oxidized state. Considering the $T_m$ reported for the mesophilic cytochromes $c_{551}$ from *Pseudomonas aeruginosa* (*51*) and the mitochondrial cytochrome *c* from horse heart (*53*), 86 and 82 °C, respectively, it is possible to infer that *Rm*cyt*c* is more thermostable; nevertheless, it should be noted that the thermostability of cytochromes *c* is in general high.

In summary, the here discussed monoheme cytochrome *c* presents the features usually observed in proteins of this kind, such as the redox potential and the visible absorption, visible circular dichroism, and EPR spectra; nevertheless it presents remarkable amino acid sequence and structural peculiarities, such as an unusual α-helix and a unique N-terminal extension, which wraps around the back of the molecule, which made it possible to describe *Rm*cyt*c* as the first member of a new class of cytochromes, so far only found in the Bacteroidetes phylum.

## ACKNOWLEDGMENT

We are grateful to Manuela Regalla from the Protein Sequence service of ITQB, to João Carita for cell growth, and to Filipa Sousa for providing the $caa_3$ oxygen reductase. We thank Dr. Carlos Frazão for advice on producing the dendrogram.

## REFERENCES

1. Bayir, H., Fadeel, B., Palladino, M. J., Witasp, E., Kurnikov, I. V., Tyurina, Y. Y., Tyurin, V. A., Amoscato, A. A., Jiang, J., Kochanek, P. M., DeKosky, S. T., Greenberger, J. S., Shvedova, A. A., and Kagan, V. E. (2006) Apoptotic interactions of cytochrome c: Redox flirting with anionic phospholipids within and outside of mitochondria. *Biochim. Biophys. Acta 1757*, 648–659.
2. Bertini, I., Cavallaro, G., and Rosato, A. (2006) Cytochrome c: Occurrence and functions. *Chem. Rev. 106*, 90–115.
3. Ambler, R. P. (1991) Sequence variability in bacterial cytochromes c. *Biochim. Biophys. Acta 1058*, 42–47.
4. Moore, G. R., and Pettigrew, G. W. (1990) *Cytochromes c. Evolutionary, Structural, and Physicochemical Aspects*, Springer-Verlag, Berlin - Heidelberg - New York.
5. Petursdottir, S. K., Hreggvidsson, G. O., Da Costa, M. S., and Kristjansson, J. K. (2000) Genetic diversity analysis of Rhodothermus reflects geographical origin of the isolates. *Extremophiles 4*, 267–274.
6. Andresson, O. S., and Fridjonsson, O. H. (1994) The sequence of the single 16S rRNA gene of the thermophilic eubacterium Rhodothermus marinus reveals a distant relationship to the group containing Flexibacter, Bacteroides, and Cytophaga species. *J. Bacteriol. 176*, 6165–6169.
7. Degryse, E., Glansdorff, N., and Pierard, A. (1978) A comparative analysis of extreme thermophilic bacteria belonging to the genus *Thermus*. *Arch. Microbiol. 117*, 189–196.
8. Arslan, E., Schulz, H., Zufferey, R., Kunzler, P., and Thony-Meyer, L. (1998) Overproduction of the *Bradyrhizobium japonicum* c-type cytochrome subunits of the cbb3 oxidase in *Escherichia coli*. *Biochem. Biophys. Res. Commun. 251*, 744–747.
9. Pereira, M. M., Carita, J. N., and Teixeira, M. (1999) Membrane-bound electron transfer chain of the thermohalophilic bacterium *Rhodothermus marinus*: A novel multihemic cytochrome bc, a new complex III. *Biochemistry 38*, 1268–1275.
10. Edman, P. B., G. (1967) A protein sequenator. *Eur. J. Biochem. 1*, 80–91.
11. Pereira, M. M., Carita, J. N., and Teixeira, M. (1999) Membrane-bound electron transfer chain of the thermohalophilic bacterium Rhodothermus marinus: Characterization of the iron−sulfur centers from the dehydrogenases and investigation of the high-potential iron−sulfur protein function by in vitro reconstitution of the respiratory chain. *Biochemistry 38*, 1276–1283.
12. McGinnis, S., and Madden, T. L. (2004) BLAST: At the core of a powerful and diverse set of sequence analysis tools. *Nucleic Acids Res. 32*, W20–25.
13. Peterson, J. D., Umayam, L. A., Dickinson, T., Hickey, E. K., and White, O. (2001) The comprehensive microbial resource. *Nucleic Acids Res. 29*, 123–125.
14. Thompson, J. D., Higgins, D. G., and Gibson, T. J. (1994) CLUSTAL W: Improving the sensitivity of progressive multiple sequence alignment through sequence weighting, position-specific gap penalties and weight matrix choice. *Nucleic Acids Res. 22*, 4673–4680.
15. Stelter, M., Melo, A. M. P., Saraiva, L. M., Teixeira, M., and Archer, M. (2007) Crystallization and X-ray analysis of *Rhodothermus marinus* cytochrome c at 1.23 Å resolution. *Protein Pept. Lett. 14*, 1038–1040.
16. Collaborative Computational Project (1994) Collaborative Computational Project, Number 4. *Acta Crystallogr. D50*, 760–763.
17. Usón, I., and Sheldrick, G. M. (1999) Advances in direct methods for protein crystallography. *Curr. Opin. Struct. Biol. 9*, 643–648.

18. Sheldrick, G. M. (2003) SHELX,University of Göttingen, Göttingen, Germany.
19. Sheldrick, G. M. (2002) Macromolecular phasing with SHELXE. *Z. Kristallogr. 217*, 644–650.
20. Caliandro, R., Carrozzini, B., Cascarano, G. L., De Caro, L., Giacovazzo, C., and Siliqi, D. (2005) Ab initio phasing at resolution higher than experimental resolution. *Acta Crystallogr. D61*, 1080–1087.
21. Morris, R. J., Perrakis, A., and Lamzin, V. S. (2002) ARP/wARP's model-building algorithms. I. The main chain. *Acta Crystallogr. D58*, 968–975.
22. Emsley, P., and Cowtan, K. (2004) Coot: Model-building tools for molecular graphics. *Acta Crystallogr. D60*, 2126–2132.
23. Sheldrick, G. M., and Schneider, T. R. (1997) SHELXL: High Resolution Refinement. *Methods Enzymol. 277*, 319–343.
24. Read, R. J. (1986) Improved Fourier coefficients for maps using phases from partial structures with errors. *Acta Crystallogr. A42*, 140–149.
25. Engh, R. A., and Huber, R. (1991) Accurate bond and angle parameters for X-ray protein structure refinement. *Acta Crystallogr. A47*, 392–400.
26. Kabsch, W., and Sander, C. (1983) Dictionary of protein secondary structure: Pattern recognition of hydrogen-bonded and geometrical features. *Biopolymers 22*, 2577–2637.
27. Vriend, G. (1990) WHAT IF: A molecular modeling and drug design program. *J. Mol. Graphics 8*, 52–56.
28. Krissinel, E., and Henrick, K. (2004) Secondary-structure matching (SSM), a new tool for fast protein structure alignment in three dimensions. *Acta Crystallogr. D60*, 2256–2268.
29. Saitou, N., and Nei, M. (1987) The neighbor-joining method: a new method for reconstructing phylogenetic trees. *Mol. Biol. Evol. 4*, 406–425.
30. Felsenstein, J. (1989) PHYLIP—Phylogeny Inference Package (Version 3.2). *Cladistics 5,* 164–166.
31. de Keyzer, J., van der Does, C., and Driessen, A. J. (2003) The bacterial translocase: A dynamic protein channel complex. *Cell. Mol. Life Sci. 60*, 2034–2052.
32. Stevens, J. M., Uchida, T., Daltrop, O., and Ferguson, S. J. (2005) Covalent cofactor attachment to proteins: cytochrome c biogenesis. *Biochem. Soc. Trans. 33*, 792–795.
33. Kelly, S. M., and Price, N. C. (2000) The use of circular dichroism in the investigation of protein structure and function. *Curr. Protein Pept. Sci. 1*, 349–384.
34. Kelly, S. M., Jess, T. J., and Price, N. C. (2005) How to study proteins by circular dichroism. *Biochim. Biophys. Acta 1751*, 119–139.
35. Yamanaka, T. (1992) *The Biochemistry of Bacterial Cytochromes*, Japan Scientific Societies Press, Tokyo.
36. Santana, M., Pereira, M. M., Elias, N. P., Soares, C. M., and Teixeira, M. (2001) Gene cluster of *Rhodothermus marinus* high-potential iron-sulfur protein: Oxygen oxidoreductase, a caa(3)-type oxidase belonging to the superfamily of heme-copper oxidases. *J. Bacteriol. 183*, 687–699.
37. Pereira, M. M., Carita, J. N., Anglin, R., Saraste, M., and Teixeira, M. (2000) Heme centers of *Rhodothermus marinus* respiratory chain. Characterization of its cbb3 oxidase. *J. Bioenerg. Biomembr. 32*, 143–152.
38. Verissimo, A. F., Pereira, M. M., Melo, A. M., Hreggvidsson, G. O., Kristjansson, J. K., and Teixeira, M. (2007) A ba3 oxygen reductase from the thermohalophilic bacterium *Rhodothermus marinus*. *FEMS Microbiol. Lett. 269*, 41–47.
39. Soulimane, T., von Walter, M., Hof, P., Than, M. E., Huber, R., and Buse, G. (1997) Cytochrome-c552 from *Thermus thermophilus*: A functional and crystallographic investigation. *Biochem. Biophys. Res. Commun. 237*, 572–576.
40. Ramachandran, G. N. S. V. (1968) Conformation of polypeptides and proteins. *Adv. Protein Chem. 23*, 283–438.
41. Hobbs, J. D., and Shelnutt, J. A. (1995) Conserved nonplanar heme distortions in cytochromes c. *J. Protein Chem. 14*, 19–25.
42. Srinivasan, V., Rajendran, C., Sousa, F. L., Melo, A. M., Saraiva, L. M., Pereira, M. M., Santana, M., Teixeira, M., and Michel, H. (2005) Structure at 1.3 Å resolution of *Rhodothermus marinus* caa(3) cytochrome c domain. *J. Mol. Biol. 345*, 1047–1057.
43. Than, M. E., Hof, P., Huber, R., Bourenkov, G. P., Bartunik, H. D., Buse, G., and Soulimane, T. (1997) *Thermus thermophilus* cytochrome-c552: A new highly thermostable cytochrome-c structure obtained by MAD phasing. *J. Mol. Biol. 271*, 629–644.
44. Bushnell, G. W., Louie, G. V., and Brayer, G. D. (1990) High-resolution three-dimensional structure of horse heart cytochrome c. *J. Mol. Biol. 214*, 585–595.
45. Beissinger, M., Sticht, H., Sutter, M., Ejchart, A., Haehnel, W., and Rosch, P. (1998) Solution structure of cytochrome c6 from the thermophilic cyanobacterium *Synechococcus elongatus*. *EMBO J. 17*, 27–36.
46. Hunte, C., Solmaz, S., and Lange, C. (2002) Electron transfer between yeast cytochrome bc(1) complex and cytochrome c: a structural analysis. *Biochim. Biophys. Acta 1555*, 21–28.
47. Muresanu, L., Pristovsek, P., Lohr, F., Maneg, O., Mukrasch, M. D., Ruterjans, H., Ludwig, B., and Lucke, C. (2006) The electron transfer complex between cytochrome c552 and the CuA domain of the *Thermus thermophilus* ba3 oxidase. A combined NMR and computational approach. *J. Biol. Chem. 281*, 14503–14513.
48. Deleted at galley stage.
49. Kumar, S., Tsai, C. J., and Nussinov, R. (2000) Factors enhancing protein thermostability. *Protein Eng. 13*, 179–191.
50. Hasegawa, J., Yoshida, T., Yamazaki, T., Sambongi, Y., Yu, Y., Igarashi, Y., Kodama, T., Yamazaki, K., Kyogoku, Y., and Kobayashi, Y. (1998) Solution structure of thermostable cytochrome c-552 from *Hydrogenobacter thermophilus* determined by 1H-NMR spectroscopy. *Biochemistry 37*, 9641–9649.
51. Nakamura, S., Ichiki, S., Takashima, H., Uchiyama, S., Hasegawa, J., Kobayashi, Y., Sambongi, Y., and Ohkubo, T. (2006) Structure of cytochrome c552 from a moderate thermophilic bacterium, *Hydrogenophilus thermoluteolus*: Comparative study on the thermostability of cytochrome c. *Biochemistry 45*, 6115–6123.
52. Uchiyama, S., Ohshima, A., Nakamura, S., Hasegawa, J., Terui, N., Takayama, S. J., Yamamoto, Y., Sambongi, Y., and Kobayashi, Y. (2004) Complete thermal-unfolding profiles of oxidized and reduced cytochromes C. *J. Am. Chem. Soc. 126*, 14684–14685.
53. Heimburg, T., and Marsh, D. (1993) Investigation of secondary and tertiary structural changes of cytochrome c in complexes with anionic lipids using amide hydrogen exchange measurements: an FTIR study. *Biophys. J. 65*, 2408–2417.

BI800999G